

Investigation of the anchor chain tension distribution and six-degree-of-freedom motion characteristics of a floating fan platform in a wind-wave basin

Xi Zhang¹, Jie Dong², Jiankang Wang¹, Guirong Lu¹, Jingyi Wei¹, Yupeng Wang¹, Guoqiang Chen^{1*}

¹Jiangsu Rudong Experimental Base, Institute of Fishery Engineering, Chinese Academy of Fishery Sciences

²Ship and Ocean Engineering, Jiangsu University of Science and Technology

Abstract

INTRODUCTION: Because of its versatility and adaptability, floating wind turbine platforms have emerged as the go-to foundation for deep sea wind power as offshore wind power production steadily expands into deeper waters.

OBJECTIVES: But the floating platform's six-degree-of-freedom motion and the anchor chain system's mechanical reaction to the combined force of wind, wave, and current are incredibly intricate, and this directly affects the platform's stability and safety.

METHODS: Under various wind, wave, flow incidence angle, and chain length conditions, the platform's six-degree-of-freedom motion characteristics and anchor chain tension distribution are carefully studied using potential flow theory, the finite element method, and the fluid-structure coupling model. The numerical simulation combined JONSWAP wave spectrum and NPD wind spectrum to conduct multi-condition analysis.

RESULTS: The results show that the incidence Angle and anchor chain configuration significantly affect the dynamic response of platform pitching and heaving.

CONCLUSION: This paper deeply discusses the platform motion response under the broken anchor chain, and puts forward the corresponding optimal design scheme.

Keywords: Floating fan plateau, Six levels of freedom of movement, Cable tension, Wind and wave coupling effect, Numerical simulation, Platformer stability

Received on 27 January 2025, accepted on 20 March 2025, published on 24 April 2025

Copyright © 2025 X. Zhang *et al.*, licensed to EAI. This is an open access article distributed under the terms of the [CC BY-NC-SA 4.0](#), which permits copying, redistributing, remixing, transformation, and building upon the material in any medium so long as the original work is properly cited.

doi: 10.4108/ew.8537

*Corresponding Author, Email: chenguoqiang1413@163.com, guoqiang_chen10@outlook.com

1. Introduction

With the continuous growth of global energy demand and attention to renewable energy, wind power generation has become one of the important means to achieve low-carbon development and alleviate energy crisis [1]. In particular, offshore wind resources have gradually become the focus of wind power development due to their richness and stability [2]. However, the construction and operation of offshore wind farms are faced with many technical challenges, among which the design and dynamic performance analysis of

floating fan platforms are important topics affecting their operational stability and safety [3]. Due to the complex coupling effect of floating platform with wind, wave and current environment, the mechanical response of its six-degree-of-freedom motion and anchor chain system is extremely complicated, further increasing the difficulty of system design and evaluation [4]. An offshore structure known as a floating wind turbine platform holds wind turbines in deep seas, increasing the potential for offshore wind energy and providing access to stronger, more reliable winds. It has dynamic cables, a mooring system, a floating

platform, and a wind turbine. Complex grid connections and hefty startup expenses are obstacles.

The development of offshore waters has progressively expanded to deep-sea regions in recent years due to the constant advancement of fan power, and the conventional fixed fan foundation is no longer adequate to satisfy the demands of these seas [5]. As a new type of deepwater wind power foundation, floating fan platform has attracted wide attention due to its flexibility, adaptability and relatively low construction cost [6]. Compared with fixed platforms, floating platforms can be installed in deeper sea areas, have certain degrees of freedom of displacement and tilt, and maintain better stability under extreme ocean conditions [7]. To improve platform stability, efficiency, and safety in harsh offshore environments, the suggested techniques for floating wind turbine platform stability—Advanced Dynamic Modeling, Adaptive Mooring System, Motion Damping and Control, and Real-Time Monitoring—strive to forecast platform motion, maintain balance, distribute loads, avoid slippage, and guarantee optimal turbine performance. As a result, a key area of current research is how to build and optimise the floating fan platform's motion response and anchor chain system to continue to operate steadily in the face of intense wind, wave, and current action [8]. The design of the anchor chain system seeks to reduce tension variations, distribute weight effectively, and enhance fatigue resistance to preserve the stability and safety of a floating platform. Motion is predicted, fluid-structure interactions are modeled, and platform design is optimised for maximum performance through dynamic response modeling.

The design of the floating fan platform is faced with many complex problems, among which the most significant challenge comes from the dynamics of fluid-structure coupling. Kinematics, dynamics, free surface, mooring system, and bottom conditions are important boundary conditions for floating platform simulations. Reliable floating platform analysis is ensured by proper application, which enhances wave load, structural response, and mooring system accuracy. A floating platform moves in six degrees of freedom—roll, heave, roll, pitch, and yaw—under the influence of wind, waves, and the surrounding environment [9]. Wave, wind, and current forces affect a floating platform's six degrees of freedom (DOF): roll, pitch, yaw, surge, sway, and heave. Turbine construction, mooring lines, and stability are all impacted by these DOFs. Accurately simulating and forecasting platform behavior while considering wave excitation, wind, and current factors requires coupled dynamic modeling. The movement of each degree of freedom will impact the platform's stability. In

addition, as the main positioning equipment of the platform, the tension distribution and stress state of the anchor chain system directly affect the motion response of the platform [10]. Under complex ocean conditions, the anchor chain system must withstand the combined forces from sea wind, waves and ocean currents. For floating wind platforms to remain stable in choppy ocean conditions, anchor chain design is essential. The difficulties include dynamic stress, environmental factors, material selection, and failure mechanisms. Innovative anchor designs, corrosion-resistant metals, frequent inspections, and redundant mooring lines are examples of mitigation techniques. One of the key issues to be solved is how to reasonably design the length, material and arrangement of the anchor chain to maintain the stability of the platform under extreme conditions [11-12]. To enhance water level monitoring systems, (Sri Harsha Grandhi, 2021) will integrate passive IoT optical fiber sensor networks with Human-Machine Interface (HMI) display modules. It helps avoid flooding and regulate the environment using Fiber Bragg Grating (FBG) sensors for real-time data display and sophisticated feature extraction. For performance measures, the resilience of the system is examined and verified [13]. Naga Sushma Allur, (2021) examines how edge computing, artificial intelligence, and machine learning may optimise resource allocation in cloud data centers. It suggests a novel load-balancing approach that strategically divides workloads between data centers and virtual machines to increase scalability, efficiency, and performance [14].

The design optimisation of the anchor chain system and the dynamic response simulation of the floating fan platform are the primary areas of current research. Dynamic response modelling is crucial for evaluating floating wind turbine platforms' durability, stability, and effectiveness in various environmental circumstances. It takes into account structural stresses as well as hydrodynamic and aerodynamic forces. The prediction of severe conditions, force coupling, and computing complexity are among the difficulties. For example, based on dynamic response analysis of potential flow theory and finite element method, the motion characteristics and cable tension distribution of floating platform under different ocean conditions are evaluated by numerical simulation [15-16]. Potential flow theory is an effective hydrodynamic modeling technique for early-stage design in offshore engineering. It has been verified using industry-standard methods and is correct for linear wave theory. However, it is restricted for harsh weather conditions, ignores viscous effects, and is incorrect for nonlinear waves. However, most of these studies were conducted under simplified conditions, ignoring the complex coupling effects of stroke, wave and current in the actual Marine environment,

and failing to fully reflect the dynamic response characteristics of the floating platform under real working conditions [17-18]. Furthermore, the anchor chain system's current design mostly relies on the anchor chain's constant length and arrangement, and a thorough investigation into the platform's reaction in the event of an anchor chain breakage is lacking [19-20]. In harsh circumstances, stability and safety are ensured by a mooring system with anchor chain breaking. Through load adjustment systems, it lowers the risk of capsizing, prevents platform loss through redundant lines, and improves safety. Advanced systems can also be subjected to fatigue study to anticipate failure from cyclic loads. Therefore, how to accurately predict the dynamic behavior of the floating platform and optimise the anchor chain system to cope with emergencies under the premise of considering complex ocean conditions is still a difficult point in the current research.

The six-degree-of-freedom motion of a floating fan platform under the combined influence of wind, wave, and current as well as the mechanical response of the anchor chain system are thoroughly examined in this paper. It is based on potential flow theory, the finite element method, and the fluid-structure coupling model. Predicting platform behavior under wind and wave stresses requires understanding fluid dynamics and rigid body motion. While multibody dynamics or kinematic equations handle rigid body motion, the fluid-structure interaction method describes fluid dynamics. FAST/OpenFAST and OrcaFlex are popular simulation tools. The research in this paper not only considers the dynamic response of the platform under normal working conditions, but also deeply discusses the stability and motion characteristics of the platform under broken anchor chain, thus providing an important reference for the design and optimisation of the floating fan platform. Floating platforms are vulnerable to anchor chain failure and platform instability because of severe weather, corrosion, overloading, and unstable seabeds. Among the mitigation strategies are dynamic positioning systems, frequent inspections, redundant mooring lines, and tension monitoring. Multi-condition testing and analysis are part of design and simulation safety. Unlike traditional studies, this paper fully considers the complex coupling effects of wind, wave and current. It comprehensively evaluates the motion characteristics of a floating fan platform under extreme ocean conditions through a combination of numerical simulation and experimental verification.

Firstly, a fan platform and anchor chain coupling system model based on Deep Wind semi-submersible floating platform is constructed in this paper. JONSWAP wave

spectrum and NPD wind spectrum simulate and analyse the motion characteristics under different incident angles and anchor chain lengths. The research results show that the incident Angle of wind and wave current significantly impact the platform's longitudinal and pitch motion, and the choice of different anchor chain lengths will also directly affect the platform's motion response and chain tension distribution [21-22]. Furthermore, this study examines the dynamic response characteristics of the plateau when the chained damage breaks under the combined influence of wind and waves, and proposes the best design strategy to address the failure of the chained damage [23-26]

2. Basic theory and analysis method

2.1 Fluid-structure coupling analysis

Fluid dynamics and platform motion are integrated in numerical simulations for floating wind platforms to forecast behavior under different circumstances. Field deployment, experimental validation, fluid-structure interaction, and model calibration are important factors. Design, functionality, and stability are enhanced in challenging ocean conditions through controlled experiments and field data validation. As can be seen from FIG. 1(a), definition $\Omega_F = R^3$ is a semi-infinite unbounded basin, $\partial\Omega_F = S_F \cup S_B \cup \Gamma_I$, and V represent a continuous three-vector water velocity field, where S_F, S_B and Γ_I represent the free liquid surface, the seabed, and the fluid-solid interface, respectively. In potential flow theory, it is assumed that the liquid is an incompressible, irrotational, inviscid ideal fluid, so there will be a velocity potential function $\varphi(x, t)$ satisfied.

$$V = \nabla\varphi \quad (1)$$

$$\varphi(x, t) = \sum_{j=1}^6 \varphi_j + \varphi_d + \varphi_k + \varphi_f \quad (2)$$

In the formula, $\varphi_j, \varphi_d, \varphi_k, \varphi_f$ is caused by the wave induced by the structure's vibration, the diffraction of the undisturbed wandering, the pressure generated by the undisturbed wandering, and the higher-order effect of the wave force. Next, the continuity equation governs the flow field.

$$\nabla^2 \varphi = 0, \Omega_F \times [0, \hat{t}] \tag{3}$$

The boundary conditions are determined by equations (2) ~ (3).

At the fluid-solid interface Γ_I :

$$\frac{\partial \varphi}{\partial n} = \dot{u} \cdot n \tag{4}$$

At the free liquid level S_F :

$$g \frac{\partial \varphi}{\partial z} + \frac{\partial^2 \varphi}{\partial t^2} = 0 \tag{5}$$

Under the sea S_B :

$$\frac{\partial \varphi}{\partial z} = 0 \tag{6}$$

\hat{t}

In the formula, \hat{t} is the time of calculation simulation, u is the displacement vector of the rigid body, where n is the unit vector and g are the acceleration of gravity, the normal line of the structural border pointing outward. Given linear and kinematic conditions, equation (5) represents a free surface condition that does not consider surface tension. La fonction potentiellement réponds à la condition de radiation: as $r \rightarrow \infty$ $\varphi \rightarrow 0$ in the far field, Anchor chain design is essential

for floating wind platforms to be structurally stable particularly in harsh conditions. Synthetic materials, active tensioning systems, redundant mooring lines, dampening devices, and optimal mooring line layout are examples of optimisations.

$\Omega_F \in R^3$

The solid region of the floating structure is Ω_S , and the boundary interface of the coupling with wind and wave

$\{d, \theta\}$

is assumed to be a rigid surface, and $\{d, \theta\}$ is defined as the translation and rotation parameters of the rigid body at its center of mass. The conservation of linear and angular momentum controls the dynamic motion of the floating structure. ($i = x, y, z$)

$$m \ddot{d}_t + \dot{c}_t d_i + k_i d_i = F_i, \partial \Omega_S [0, \hat{t}] \tag{7}$$

$$I_{ij}^\theta \ddot{\theta}_{ij} + c_i^\theta \dot{\theta}_i + k_i^\theta \theta_i = M_i, \partial \Omega_S [0, \hat{t}] \tag{8}$$

And the initial conditions are:

$$\{\dot{d}, \dot{\theta}\}_{t=0} = \{\dot{d}_0, \dot{\theta}_0\} \tag{9}$$

$$\{d, \theta\}_{t=0} = \{d_0, \theta_0\} \tag{10}$$

Where m, c_i, k_i, c_i^θ and k_i^θ are the total mass, damping and stiffness coefficients of translational freedom and damping and stiffness coefficients of rotational freedom, respectively. Meanwhile, I_{ij}^θ is defined as the moment of inertia relative to the position of the center of mass, where the vectors representing the external force and moment are, respectively, F and M .

$$F = F_{sv}(t) + F_c(t) + F_w(t) + F_t(t) + F_h(t) + F_d(t) + F_{wf}(t) \tag{11}$$

$$M = \int_{\Gamma_1} r \times F ds \tag{12}$$

Here, $F_{sv}(t)$ represents the slowly changing drift force, $F_c(t)$ represents the drag force of water flow, $F_w(t)$ represents the wind resistance, $F_t(t)$ represents the mooring force, $F_h(t)$ represents the hydrostatic pressure, $F_d(t)$ represents the

resistance force, $F_{wf}(t)$ represents the wave frequency force, and r is the position vector relative to the center of mass. The Froude-Krylov force resulting from undisturbed waves, the diffraction force generated by the structure itself influencing the wave density, and the radiation force formed by the wave induced by the vibration of the structure make up the majority of the first-order linear wave force among them. Ultimately, drift motion and wave frequency motion are combined to generate the floating structure's overall response.

2.2 Mooring analysis

Concerning hydrodynamic pressure, dead weight, inertia force, and traction force, the construction of the L-length cable chain is thin and pliable. According to Figure 1(b), the nonlinear differential equation of motion for the differential element d_l of the anchor chain is governed by the translation and rotation equilibrium equations.

$$(m_c + m_a) \frac{\partial \dot{u}_c}{\partial t} = \frac{\partial T_c}{\partial s} + (1 + \gamma) F_c \quad (13)$$

$$\frac{\partial M_c}{\partial s} - r_t \times (1 + \gamma) F_c \quad (14)$$

And the coordination equation:

$$\frac{\partial \dot{u}_c}{\partial s} = \frac{\partial}{\partial t} [(1 + \gamma) r_t] \quad (15)$$

The boundary conditions are determined by:

At $s = 0$ (seabed) :

$$\dot{u}_c = 0, \vartheta_c = \vartheta_c^B \quad (16)$$

At $s = L$ (anchor point) :

$$\dot{u}_c = \dot{d}_p, \vartheta_c = \vartheta_c^P \quad (17)$$

In the formula, the mass of the anchor chain per unit length is known as m_c , m_a is the additional mass of the sea water, The arc length of the untensed anchor chain is denoted by s , and the velocity vector is \dot{u}_c , γ is the strain, r_t is the vector tangent to the center line of the anchor chain, M_c is the resultant moment, F does unit weight cause the external load per unit weight, and F_n , F_t and F_q are the normal, tangential and vice normal dragging forces. The unit vector q is defined in the normal direction by $q = \dot{u}_c \times \tau / |\dot{u}_c \times \tau|$, where τ is the tangential unit vector.

The finite element approach approximates the dynamic response of the rigid floating platform and mooring chain, while the boundary element method, interpolated by equations (3) through (6), controls the potential flow motion. For the dynamic motion analysis of rigid body, the platform structure is divided into grids on the surface of the underwater part of the platform. According to the three-dimensional source and sink distribution theory, the surface element numerical calculation method is adopted to solve the load on the platform in waves. The dynamic force of sea breeze and sea current on the floating platform is calculated by multiplying the wind and flow force coefficients by the square of the corresponding wind and flow velocity. Platform movements are greatly impacted by wind turbine thrust and torque in high wind situations. Optimising platform stability and guaranteeing turbine performance in harsh conditions requires understanding these impacts. Higher wind speeds provide greater thrust, which increases the structure's bending moments and stresses. A finite number of line units make up each mooring line. Uneven tension distribution, dynamic load fluctuations, and nonlinear behavior are some of the difficulties that mooring line coupling encounters. Damping processes, adaptive mooring control, and tension balance are achieved through hydrodynamic models, coupled aero-hydro-elastic models, and quasi-static vs. dynamic models. The time integral of the motion equation is calculated using the two-step prediction approach. The Euler-Lagrange coupling method handles the interaction between the motion of the rigid structure and the fluid, and the numerical simulation is performed using an alternating iteration method. The floating structure and mooring chain are subject to external force and moment from the hydrodynamic pressure. Until the interleaving computation is repeated until the

predetermined calculation duration of three hours, the wet surface of the fluid-to-structure interface varies continuously with the rigid body movement of the floating structure.

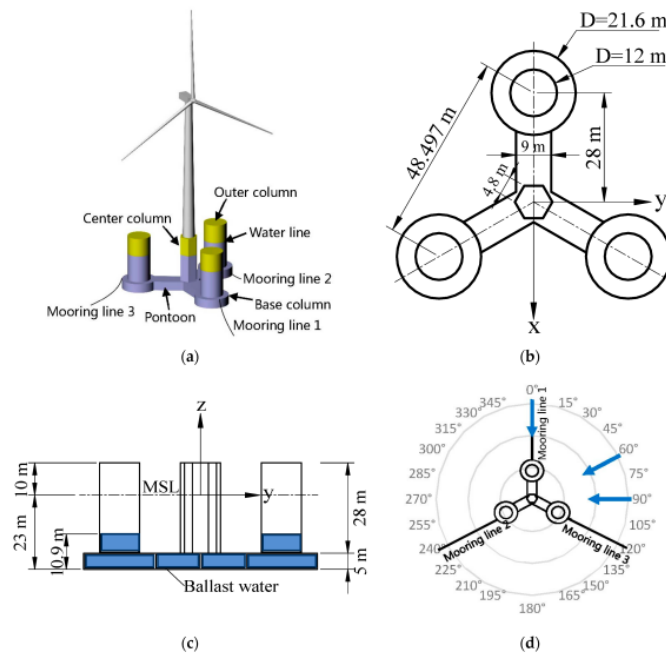


FIG. 1 Structural force analysis of semi-submersible mooring platform

3 Calculation model

3.1 Fan and floating platform model

Deep Wind semi-submersible floating platform is used for floating platform mining. Wave and wind loads affect how floating platforms behave; high wind speeds increase aerodynamic thrust and torque, while waves provide

hydrodynamic forces that cause complicated motion responses and resonance effects, reducing turbine performance. The specific parameters and structure are shown in Table 1 and Figure 2. The upper fan adopts a 5 MW three-blade vertical axis wind turbine, which acts on the floating platform as a concentrated mass. The height of the center of mass and buoyancy are determined by the position of the relative free water surface; Table 2 gives the specific values.

Table 1 Geometric parameters of floating platform

Floating platform geometry /m	Parameter value
Draft depth of floating platform	20
Height above the surface of the main column	10
Height above the water line of the top surface of the column	12

Distance between three partial columns	50
Partial column (upper) height	25
Partial column (lower) height	7
Height below the surface of the top of the column	15
Diameter of the main column	6.5
Partial column (upper) diameter	12
Partial column (lower) diameter	25
Support rod diameter	1.5

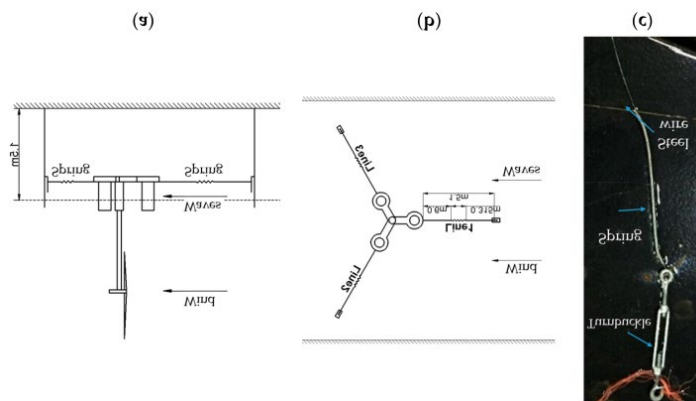


FIG. 2 Calculation model of floating platform

Table 2 Floating platform and fan characteristics

Floating platform and fan characteristics	Parameter value
Platform mass, including ballast tanks m_1/kg	1.345×10^7
Moment of inertia about the X-axis of the platform concerning the center of mass $I_{xx}/(kg \cdot m^2)$	6.825×10^9
Moment of inertia about the Y-axis of the platform concerning the center of mass $I_{yy}/(kg \cdot m^2)$	6.825×10^9
Moment of inertia of the platform about the Z-axis concerning the center of mass $I_{zz}/(kg \cdot m^2)$	1.228×10^{10}
Rotor mass, including blades, supports and towers, m_2/kg	3.151×10^5
Height of center of mass of floating platform (below water surface line) /m	13.460

3.2 Mooring structure

3.2.1 Normal status

Figure 3(a) depicts the mooring setup in typical circumstances. The mooring system consists of three identical anchor chains. The angle between the adjacent horizontal plane is 120° , and there is a catenary structure between the anchor point and the seafloor. The sea depth is 200 m, the cable length is 835.5 m, the diameter is 0.0766 m, the equivalent mass density of the cable is 113.35 kg/m, the equivalent axial stiffness of the cable is 753.6 MN, the breaking force of the cable is 10 MN, and the hydrodynamic

additional mass coefficient is 1.0. The structural damping is added to the structural calculation in the form of critical damping, and the effects of extra mass, hydrostatic stiffness, mooring stiffness and structural inertia mass are considered.

3.2.2 Broken states

If the anchor system is under the action of wind, wave and current for a long time, its anchor chain will be subjected to the pull action of the platform and wear in the seabed, which will cause damage or even break. At this time, it is necessary to consider that the mooring system can have sufficient positioning capability to ensure the stability and safety of the floating platform. Real-time tension monitoring,

load and fatigue analysis, and mooring system modeling are the methods used in this work to prevent anchor chain failure and platform instability in floating platforms. It also employs aero-hydro-elastic modeling to replicate real-world situations and study wind-wave interactions to optimise ballast distribution and mooring tension feedback loops. Because the

mooring system with three anchor chains is not robust enough to resist breaking the anchor chain, the mooring system in Figure 3(b) is designed. The anchor chain parameters of the mooring system, which consists of six identical anchor chains in the form of a catenary, are the same as they are in the normal state.

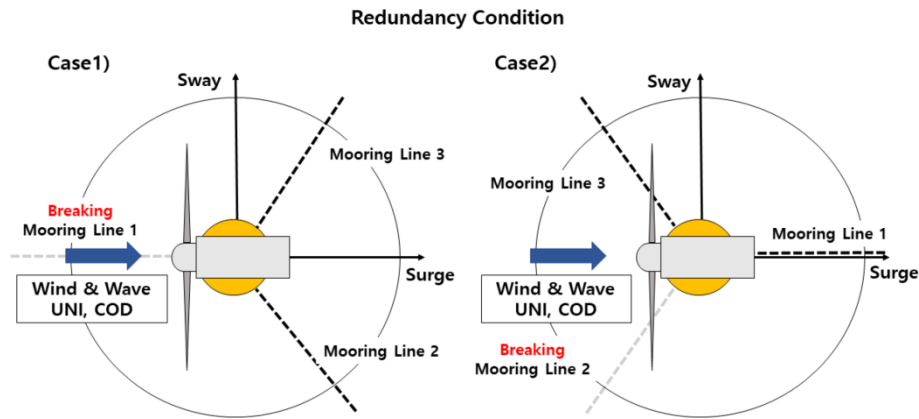


FIG. 3 Mooring system layout under normal and broken conditions

3. 3 Wind wave current model

The wave spectrum represents the entire wave energy propagating as a wave field at a given time and shows how wave energy is distributed with frequency. The JONSWAP spectrum is a commonly used wave spectrum that may be applied to sea states broken down into several sine wave components. The JONSWAP and NPD spectra support fatigue and stability evaluations for floating platforms, enhance hydrodynamic models, and predict irregular waves. Additionally, they support the optimisation of control systems to increase stability. This connection guarantees durability and efficiency by enabling real-world offshore wind turbine design improvement. It is an empirical formula for irregular wave energy distribution and frequency. It is predicated on the idea that the wave reaches an equilibrium condition, or that a fully formed wave forms under a sizable area in a stable sea breeze over an extended period. The energy density $S(w)(m^2/Hz)$ of the JONSWAP spectrum is defined as follows.

$$S(w) = \frac{\alpha g^2}{w^5} \exp\left[-\frac{5}{4}\left(\frac{w_m}{w}\right)^4\right] \gamma^{\exp\left[-\frac{(w-w_m)^2}{2\sigma^2 w_m^2}\right]} \quad (18)$$

In equation (18), γ is the factor of spectral peak elevation, and the average value is 3.3. Here, 1.7 is used. w_m is the peak frequency; σ is the peak shape coefficient, its value is:

$$\begin{cases} \sigma = 0.007, w \leq w_m \\ \sigma = 0.009, w > w_m \end{cases} \quad (19)$$

The coefficient α is a function of the dimensionless wind region, namely:

$$\alpha = 0.076 \left(\frac{gx}{U^2}\right)^{-0.22} \quad (20)$$

In Formula (20), the wind speed at a height of 10 meters above the sea surface is represented by U , while the wind zone's length is represented by x .

The temporal history of irregular waves for a particular spectrum can be calculated via linear superposition of

harmonic components. $\eta(x, t)$ wave height is expressed as follows.

$$\eta(x, t) = \frac{1}{2} \sum_{n=1}^N A_n \cos(k_n x - 2\pi f_n t + \varphi_n) \tag{21}$$

Equation (21) respectively represents the amplitude, wave number, frequency and phase Angle of the wave. The relationship between the energy density and the amplitude A_n of the J-order wave component.

$$\frac{A_j^2}{2} = S(w_j) \frac{w_{\max} - w_{\min}}{N} \tag{22}$$

The frequency interval is equally divided into 40 parts. The minimum and maximum frequencies of JONSWAP spectrum simulation calculation are 0.1 Hz and 0.7 Hz respectively.

Because the Marine mooring floating platform structure is more sensitive to low frequency response, and the NPD wind spectrum has more energy concentrated in the low frequency, the NPD spectrum is chosen as the ocean wind spectrum. The energy density of the NPD spectrum $S(w)(m^2/Hz)$ is defined below.

$$S(f) = \frac{320(\frac{U_{10}}{10})^2(\frac{z}{10})^{0.45}}{(1 + \tilde{f}^{0.468})^{3.561}} \tag{23}$$

$$\tilde{f} = \frac{172f(\frac{z}{10})^{\frac{2}{3}}}{(\frac{U_{10}}{10})^{\frac{3}{4}}} \tag{24}$$

Where, $S(f)$ is wind spectral energy density, U_{10} is the average hourly wind speed at a relative altitude of 10 m, m/s.

ANSYS/AQWA can invoke the wind and wave spectra it supports. Ocean waves adopt JONSWAP spectrum, with $\gamma = 1.7$ $H_s = 2.5m$ peak elevation factor meaningful wave height $T_p = 8.9s$ and peak period Figure 4 (a) shows the related spectral energy density curve with frequency. Sea breeze uses the NPD spectrum; Figure 4(b) displays the curve of spectral energy density changing with frequency. At a relative height of 10 m, the average hourly wind speed is 20 m/s. The current has a constant flow of 0.8 m/s.

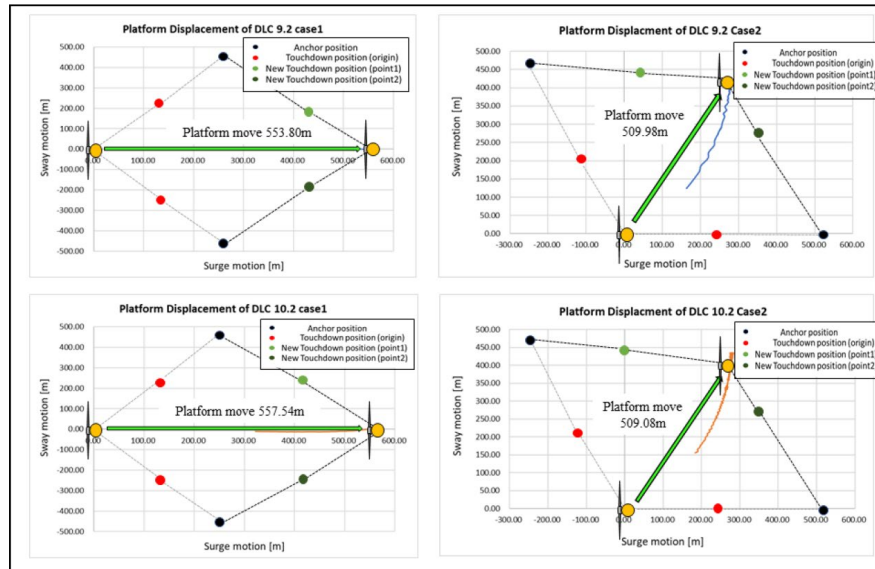


FIG. 4 JONSWAP wave spectrum and NPD wind spectrum models

4. Verify the example

4.1 Grid accuracy verification

The second-order mean drift force can be found using two different approaches: the pressure-motion integral method and the far-field integral method, both of which are based on momentum-energy conservation. The former uses the great degree of momentum and energy conservation accuracy to calculate the second-order mean drift force from the fluid around the floating body. Using perturbation expansion, the second order fluid pressure is acquired; the second order average drift force is then obtained by integrating the second order wave pressure along the object's wet surface. Grid refinement lowers errors and improves predictions by capturing intricate phenomena like platform motion and wave loading. But it decreases profits and raises

computational costs. Studies on grid independence solidify findings.

The floating platform's computing unit has a grid side length of 0.4 meters. Figure 5 displays the computation results of the near field and far field methods. It monitors important parameters and evaluates accuracy using simulations on different meshes. Grid independence is attained when result variation is smaller than 2–5%. It employs both near-field and far-field validation. Error estimate is done via Richardson extrapolation. Additionally, they prioritise computational efficiency by using adaptive mesh refinement to balance cost and accuracy. The two curves are essentially consistent, suggesting that the wet surface's grid precision is adequate to guarantee the accuracy of the findings.

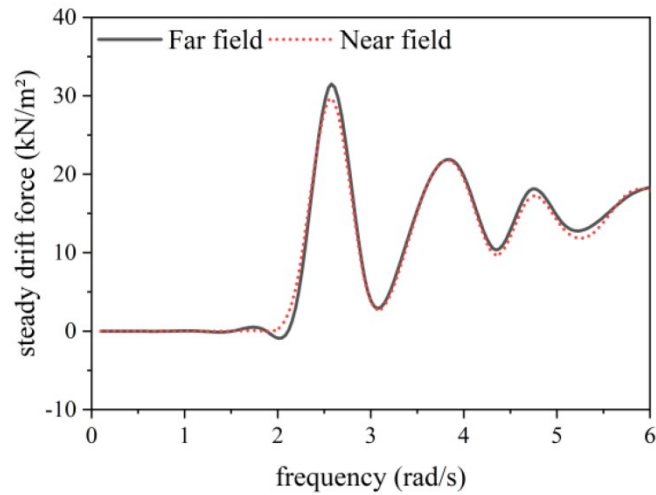


FIG. 5 Comparison of calculation results of mean drift force by far field method and near field method

4. 2 Self-vibration period verification

The six-degree-of-freedom motion of the structure's natural vibration period can be ascertained using the floating platform's free attenuation motion. In deep-sea conditions, the 6-degree-of-freedom (6DOF) motion analysis is essential for improving the robustness and dependability of floating wind platforms. The platform's whole motion under wind, waves, and currents offers advantages such as precise dynamic forecast, optimised mooring systems, platform stability,

improved turbine performance, and structural integrity. Figure 6 depicts the semi-submersible floating platform's free attenuation motion as simulated by numerical simulation. Table 3 compares the natural vibration period of the floating platform as determined by this paper's simulation results and the actual results. The computation approach used in this work is reliable, as evidenced by the relative inaccuracy of the two values within 5%.

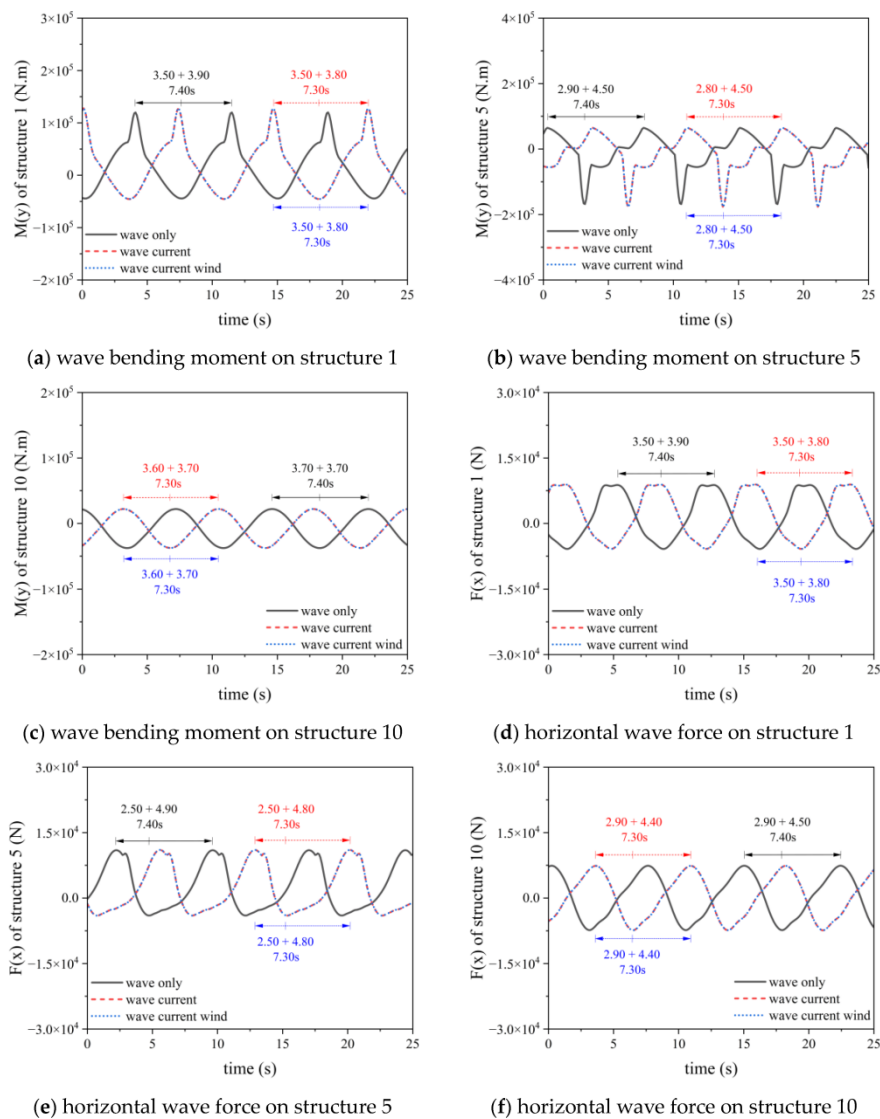


FIG. 6: Semi-submersible floating platform's free attenuation motion

Table 3 Comparison of calculation results of natural vibration period

Movement	Scholar cycle /s	This text period /s	Relative error /%
Surge	113.13	115.00	1.61
Sway	113.13	115.00	1.61
Heaving	17.02	17.30	1.51
Rolling	20.66	21.86	4.66

Pitch	20.66	21.30	3.07
Yawing	80.42	80.80	0.44

4.3 Influence of Angle change of incoming flow

Because floating structures are rarely affected by unidirectional waves, numerical simulation of wave models in only one direction cannot capture the essence of the actual hydrodynamic interaction problem. It is considered that wind and wave load act on the floating fan and its foundation platform at a series of incidence angles. The semi-submersible floating platform exhibits symmetry about the X-axis, allowing the incident wave to spin at intervals of 22.5° from 0° to 180° along the X-axis. This allows for analysing

the floating platform's sluggish motion while accounting for the second-order force. Figure 7 shows the average pitch and pitch displacement amplitudes at different incident angles of wind wave flow. Since both surge and pitch are dislocations along the longitudinal direction, the component force of wind and wave flow along the longitudinal direction is the largest at 0° and 180°. When the break increases at 90°, the displacement of surge and pitch decreases continuously. When the displacement amplitude reaches the minimum value close to 0 at 90°, and then gradually increases with the incidence direction from 90° to 180°. The displacement of the pitch and the pitch is also growing.

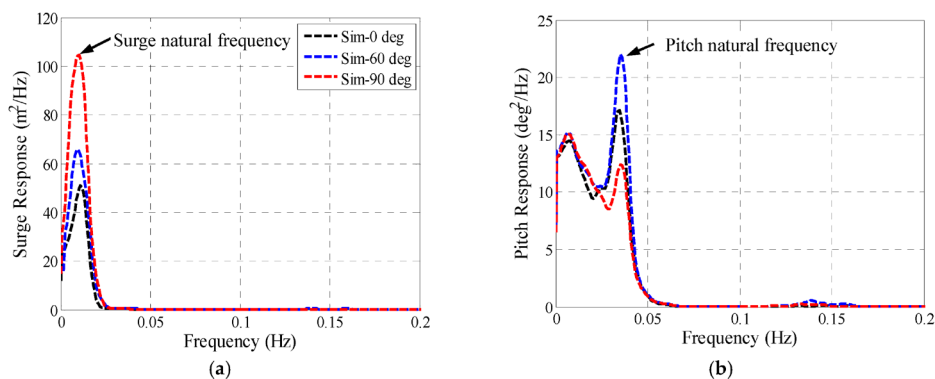


FIG. 7 Motion displacement amplitude of floating platform under different incident angles

The mooring chain tension at various storm flow incidence angles is displayed in FIG. 8(a). When the incidence angle is 0°, the anchor tension (anchor chain 2) on the side facing the waves is at its maximum. As the incident angle increases, the wave-facing side's anchor tension gradually decreases while the opposite side's anchor tension (anchor chain 1, 3) gradually increases. Altering the incidence angle will significantly impact the anchor chain's tension distribution and, in turn, the stiffness of the mooring system.

Pitching motion will be inhibited and displacement will be larger due to the chain tension created by the floating platform's displacement. Because when pulled by increasing

displacement, these three chains will be lifted from the sea floor, thereby increasing the suspension length of the chain, this process will create more tension on the chain to inhibit the platform's pitching and rolling. As illustrated in FIG. 8(a), the displacement scalar of the surge and pitch concerning the anchor chain 2 decreases as the incidence Angle increases from 0° to 180°. This is followed by a decrease in anchor chain tension, a decrease in the anchor chain's suspension length, and an increase in the length of the lying chain on the seabed [see FIG. 8(b)]. The length of the lying chain exhibits an overall decreasing trend, the anchor chain's tension increases, and the anchor chain's suspension length grows to limit the displacement.

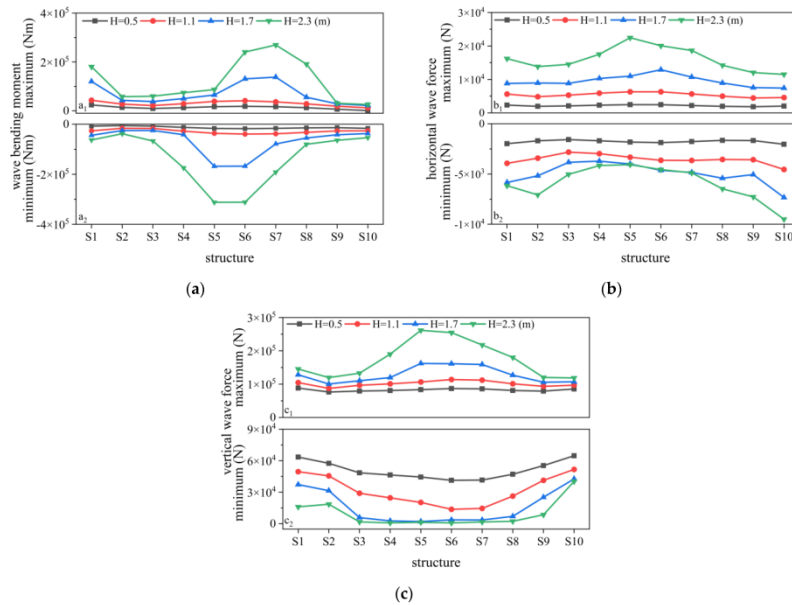


FIG. 8 Stress characteristics of mooring chain at different incidence angles

4. 4 Influence of different anchor chain lengths

Since the stress state of the floating platform is relatively stable when the incident Angle is 45° , the influence of the change of anchor chain length on the displacement change of pitching and rolling is considered when the incident Angle is 45° .

The floating platform's surge, pitch displacement, and cable tension are displayed in Figure 9 for various cable lengths. The surge displacement increases with the anchor chain's length while the anchor chain's tension decreases. Because the external load on the floating platform is fixed when the direction of wind and wave flow is fixed, its motion displacement is affected by mooring stiffness and binding force. Table 4 shows the mooring binding force under different anchor chain lengths. Under different cable lengths, the binding force of mooring system on the surge is unchanged, and it has little effect on the displacement of the surge under different cable lengths. The anchor chain tension will directly affect the anchor chain stiffness. When the anchor chain length is small, the anchor chain tension is

larger, the corresponding mooring stiffness is larger, and the displacement constraint on the floating platform is stronger. As shown in Figure 9, as the length of the anchor chain increases, the mooring stiffness and tension continually decrease. When the external load and mooring binding force are fixed, the reduction of mooring stiffness will weaken the constraint of mooring on the longitudinal displacement. As a result, as the anchor chain's length increases, so will the floating platform's surge.

The displacement amplitude of pitch will decrease with increasing anchor chain length because of the combined effects of mooring stiffness and mooring binding force under certain external loads. As shown in Table 4, when the anchor chain length is 865 m, the pitching mooring binding force of the floating platform is 2.25 times that of 825 m. It is evident that as the length of the anchor chain increases, the pitching mooring binding force would also rise noticeably. It can be seen that with the increase of the anchor chain length, although the mooring stiffness will decrease, the mooring pitch binding force will increase significantly. Since the binding force currently affects pitch more than mooring stiffness, the floating platform's pitch displacement amplitude will decrease as anchor chain length increases.

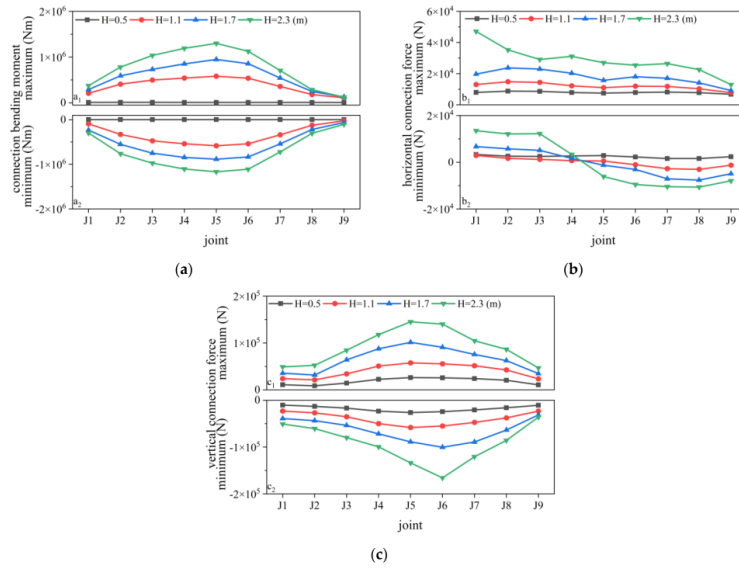


FIG. 9 Motion characteristics of floating platform under different anchor chain lengths

Table 4 Mooring binding force under different anchor chain lengths

Cable length	825m	835m	845m	855m	865m
Surge /N	3.2×10^5				
Pitch ($N \cdot m$)	2.4×10^6	3.3×10^6	4.1×10^6	4.8×10^6	5.4×10^6

5. Conclusions

In this paper, numerical simulation and experiment systematically study the kinematic characteristics and anchor chain tension distribution of the floating fan platform under the coupled environment of wind, wave and current. Under the combined action of wind, wave, and current, the floating fan platform exhibits significant six-degree-of-freedom motion, with the platform's pitch, roll, and yaw motion being the most susceptible to external factors. Especially under strong wind and wave conditions, the motion response of the platform is significantly enhanced, showing nonlinear motion characteristics. The experiment demonstrates that the anchor chain tension at various platform positions exhibits clear dynamic changes, and that the front-end anchor chain tension load increases when the wind and waves combine to create strong winds and high flow rates. In particular, these

conditions may put the system's stability at risk due to the violent fluctuations in the anchor chain tension. To guarantee the platform's stability and safety, the coupling impact of environmental load must be carefully considered during the anchor chain design process.

Declarations Funding

There is no specific funding to support this research.

Conflict of Interest

The authors declare that they have no conflicts of interest regarding this work.

Data Availability

All data generated or analysed during this study are included in the manuscript.

Code Availability

Not applicable.

Author Contributions

All Author is contributed to the design and methodology of this study, the assessment of the outcomes, and the writing of the manuscript.

References

- [1] Feng, X., Lin, Y., Gu, Y., Li, D., Chen, B., Liu, H., & Sun, Y. (2023). Preliminary stability design method and hybrid experimental validation of a floating platform for 10 MW wind turbine. *Ocean Engineering*, 285, 115401. <https://doi.org/10.1016/j.oceaneng.2023.115401>
- [2] Stansby, P., & Li, G. (2024). A wind semi-sub platform with hinged floats for omnidirectional swell wave energy conversion. *Journal of Ocean Engineering and Marine Energy*, 10(2), 433-448. <https://doi.org/10.1007/s40940-024-00199-1>
- [3] Zhou, B., Hu, J., Wang, Y., Jin, P., Jing, F., & Ning, D. (2023). Coupled dynamic and power generation characteristics of a hybrid system consisting of a semi-submersible wind turbine and an array of heaving wave energy converters. *Renewable Energy*, 214, 23-38. <https://doi.org/10.1016/j.renene.2023.03.064>
- [4] Guo, J., Liu, M., Fang, Z., Xiao, L., Chen, W., & Pan, X. (2024). Motion and mooring load responses of a novel 12 MW semi-submersible floating wind turbine: An experimental study. *Journal of Offshore Mechanics and Arctic Engineering*, 1-26. <https://doi.org/10.1115/1.4053034>
- [5] Meng, F., Lio, W. H., Pegalajar-Jurado, A., Pierella, F., Hofschulte, E. N., Santaya, A. G., & Bredmose, H. (2023). Experimental study of floating wind turbine control on a TetraSub floater with tower velocity feedback gain. *Renewable Energy*, 205, 509-524. <https://doi.org/10.1016/j.renene.2023.08.031>
- [6] Zou, Y., Liu, H., Liu, X., & Yang, X. D. (2024). Patent Technology of Shipborne Stabilized Platform. *Recent Patents on Engineering*, 18(4), 92-112. <https://doi.org/10.2174/1574892818666231002124305>
- [7] Lin, J., Wang, Y., Duan, H., Liu, Y., & Zhang, J. (2023). A scaled wind turbine model-based aerodynamic testing apparatus for offshore floating wind turbines. *Journal of Marine Engineering & Technology*, 22(6), 263-272. <https://doi.org/10.1080/20464177.2023.1961067>
- [8] Bergua, R., Wiley, W., Robertson, A., Jonkman, J., Brun, C., Pineau, J. P., ... & Conway, O. (2023). OC6 project Phase IV: validation of numerical models for novel floating offshore wind support structures. *Wind Energy Science Discussions*, 2023, 1-36. <https://doi.org/10.5194/wes-2023-104>
- [9] Huo, F. L., Luo, P., Nie, Y., Zhao, Y. P., Li, M. Y., & Xu, S. (2024). Structural Strength Study of A Floating Wind Turbine Under Freak Waves Through the CFD-FEA Method. *China Ocean Engineering*, 1-15. <https://doi.org/10.3969/j.issn.1005-9865.2024.03.004>
- [10] Gay Neto, A., Martins, G. R., do Amaral, G. A., & Franzini, G. R. (2024). Numerical methodology to model offshore systems composed of slender structures. *Archive of Applied Mechanics*, 1-31. <https://doi.org/10.1007/s00419-024-01988-0>
- [11] Kourani, A., & Daher, N. (2023). Three-dimensional modeling of a tethered UAV–buoy system with relative-positioning and directional surge velocity control. *Nonlinear Dynamics*, 111(2), 1245-1268. <https://doi.org/10.1007/s11071-023-07968-w>
- [12] Li, X. (2024). Enhancing University Physical Education Through Data-Driven Reform of Sports Club Systems. *Journal of Combinatorial Mathematics and Combinatorial Computing*, 119, 13-22. <https://doi.org/10.1305/jcmc-119-1-13>
- [13] Sri, H.G. (2021). Integrating HMI display module into passive IoT optical fiber sensor network for water level monitoring and feature extraction. *World Journal of Advanced Engineering Technology and Sciences*, 02(01), 132–139.
- [14] Naga, S.A. (2021). Optimising Cloud Data Center Resource Allocation with a New Load-Balancing Approach. *International Journal of Information Technology & Computer Engineering*, 9(2), ISSN 2347–3657.
- [15] Xie, T., Huang, L., Guo, Y., & Ou, Y. (2023). Modeling and simulation analysis of active heave compensation control system for electric-driven marine winch under excitation of irregular waves. *Measurement and Control*, 56(5-6), 1004-1015. <https://doi.org/10.1177/00202940231179059>
- [16] Jiang, M., Qiao, G., Chen, J., Huang, X., Zhang, L., Wen, Y., & Zhang, Y. (2023). Dynamic Response Analysis of Semi-Submersible Floating Wind Turbine with Different Wave Conditions. *Energy Engineering*, 120(11), 2531-2545. <https://doi.org/10.1080/01998595.2023.2227569>
- [17] Hegazy, A., Naaijen, P., Leroy, V., Bonnefoy, F., Mojjallzadeh, M. R., Pérignon, Y., & van Wingerden, J. W. (2024). The potential of wave feedforward control for floating wind turbines: a wave tank experiment. *Wind Energy Science*, 9(8), 1669-1688. <https://doi.org/10.5194/wes-9-1669-2024>
- [18] Schulz, C. W., Netzband, S., Knipper, P. D., & Abdel-Maksoud, M. (2024). Low Uncertainty Wave Tank Testing and Validation of Numerical Methods for Floating Offshore Wind Turbines. *Wind Energy Science Discussions*, 2024, 1-30. <https://doi.org/10.5194/wes-2024-12>
- [19] Ren, Z., Huang, Z., Zhao, T., Wang, S., Sun, Y., Chen, H., & Fang, N. (2024). Dynamic Modelling and Experimental Analysis of an Offshore Crane Payload Positioning System with a Parallel Cable-Driven Method. *Polish Maritime Research*, 31(2), 29-45. <https://doi.org/10.2478/polmar-2024-0031>
- [20] Altay, A., & Mirici, İ. H. (2024). EFL Instructors' Implementations of 21st Century Skills in Their Classes. *International Journal for Housing Science and Its Applications*, 45(2), 37-46. <https://doi.org/10.5479/ijhsa-45-2-37>
- [21] Wu, Y. (2024). Exploration of the Integration and Application of the Modern New Chinese Style Interior Design. *International Journal for Housing Science and Its Applications*, 45(2), 28-36. <https://doi.org/10.5479/ijhsa-45-2-28>
- [22] Chen, P. (2024). Research on Business English Approaches from the Perspective of Cross-Cultural Communication Competence. *International Journal for Housing Science and Its Applications*, 45(2), 13-22. <https://doi.org/10.5479/ijhsa-45-2-13>

- [23] Behrens de Luna, R., Perez-Becker, S., Saverin, J., Marten, D., Papi, F., Ducasse, M. L., ... & Paschereit, C. O. (2024). Quantifying the impact of modeling fidelity on different substructure concepts for floating offshore wind turbines–Part 1: Validation of the hydrodynamic module Blade-Ocean. *Wind Energy Science*, 9(3), 623-649. <https://doi.org/10.5194/wes-9-623-2024>
- [24] Ghozlane, M., & Najjar, F. (2024). Nonlinear analysis of a floating offshore wind turbine with internal resonances. *Nonlinear Dynamics*, 112(3), 1729-1757. <https://doi.org/10.1007/s11071-024-08533-x>
- [25] Konispoliatis, D. N. (2024). Floating Oscillating Water Column Wave Energy Converters: A Review of Developments. *Journal of Energy and Power Technology*, 6(1), 1-29. <https://doi.org/10.1155/2024/1054123>
- [26] Sun, K., Xu, Z., Li, S., Jin, J., Wang, P., Yue, M., & Li, C. (2023). Dynamic response analysis of floating wind turbine platform in local fatigue of mooring. *Renewable Energy*, 204, 733-749. <https://doi.org/10.1016/j.renene.2023.08.030>